Monthly Notices
of the
ROYAL ASTRONOMICAL SOCIETY

MNRAS **473,** 5113–5125 (2018)
Advance Access publication 2017 October 9

doi:10.1093/mnras/stx2622

The UKIRT Hemisphere Survey: definition and *J*-band data release

S. Dye,[1⋆] A. Lawrence,[2] M. A. Read,[2] X. Fan,[3] T. Kerr,[4] W. Varricatt,[4] K. E. Furnell,[5] A. C. Edge,[6] M. Irwin,[7] N. Hambly,[2] P. Lucas,[8] O. Almaini,[1] K. Chambers,[9] R. Green,[3] P. Hewett,[7] M. C. Liu,[9] I. McGreer,[3] W. Best,[9] Z. Zhang,[9] E. Sutorius,[2] D. Froebrich,[10] E. Magnier,[9] G. Hasinger,[9] S. M. Lederer,[11] M. Bold[12] and J. A. Tedds[13]

[1]*School of Physics and Astronomy, Nottingham University, University Park, Nottingham NG7 2RD, UK*
[2]*Institute for Astronomy, Blackford Hill, Edinburgh EH9 3HJ, UK*
[3]*Department of Astronomy/Steward Observatory, 933 North Cherry Avenue, Tucson, AZ 85721-0065, USA*
[4]*UKIRT, 660 N. A'ohōkū Place, University Park, Hilo, HI 96720, USA*
[5]*Astrophysics Research Institute, LJMU, IC2, Liverpool Science Park, 146 Brownlow Hill, Liverpool L3 5RF, UK*
[6]*Department of Physics, University of Durham, South Road, Durham DH1 3LE, UK*
[7]*Institute of Astronomy, Madingley Road, Cambridge CB3 0HA, UK*
[8]*School of Physics, Astronomy and Mathematics, University of Hertfordshire Hatfield, Hertfordshire AL10 9AB, UK*
[9]*Institute for Astronomy, University of Hawaii, 2680 Woodlawn Drive, Honolulu, HI 96822, USA*
[10]*Centre for Astrophysics and Planetary Science, University of Kent, Canterbury CT2 7NH, UK*
[11]*NASA JSC, Mail Code: XI, 2101 NASA Parkway, Houston, TX 77058, USA*
[12]*Lockheed Martin Space Systems Company, 1111 Lockheed Martin Way, Sunnyvale, CA 94089, USA*
[13]*Department of Physics and Astronomy, University of Leicester, Leicester LE1 7RH, UK*

Accepted 2017 October 3. Received 2017 September 29; in original form 2017 August 1

ABSTRACT

This paper defines the UK Infra-Red Telescope (UKIRT) Hemisphere Survey (UHS) and release of the remaining ∼12 700 deg^2 of *J*-band survey data products. The UHS will provide continuous *J*- and *K*-band coverage in the Northern hemisphere from a declination of 0° to 60° by combining the existing Large Area Survey, Galactic Plane Survey and Galactic Clusters Survey conducted under the UKIRT Infra-red Deep Sky Survey (UKIDSS) programme with this new additional area not covered by UKIDSS. The released data include *J*-band imaging and source catalogues over the new area, which, together with UKIDSS, completes the *J*-band UHS coverage over the full ∼17 900 deg^2 area. 98 per cent of the data in this release have passed quality control criteria. The remaining 2 per cent have been scheduled for re-observation. The median 5σ point source sensitivity of the released data is 19.6 mag (Vega). The median full width at half-maximum of the point spread function across the data set is 0.75 arcsec. In this paper, we outline the survey management, data acquisition, processing and calibration, quality control and archiving as well as summarizing the characteristics of the released data products. The data are initially available to a limited consortium with a world-wide release scheduled for 2018 August.

Key words: catalogues – surveys – infrared: general.

1 INTRODUCTION

Large area surveys play a fundamental role in astronomy. They are an efficient use of resources; in Euclidean space, a shallower and wider area survey explores a larger volume than a deeper and narrower one for the same total exposure time. They represent a basic point of reference, providing the statistical samples needed to address many intrinsically large angular area problems in astronomy such as studying the structure of the Milky Way and investigating the global structure of the Universe. Large area surveys are also a source of unexpected and serendipitous discoveries of rare and new classes of objects, such as high-redshift quasars (see Wang et al. 2017; Yang et al. 2017), ultra-cool brown dwarfs and free-floating planets (see for example Liu et al. 2013; Marocco et al. 2014). Full-sky or near full-sky survey coverage brings about the capability of retrospective

⋆ E-mail: simon.dye@nottingham.ac.uk

identification of sources, for example following a rare event or to find counterparts to sources detected at longer wavelengths where resolution is poor.

This paper defines the United Kingdom Infra-Red Telescope (UKIRT) Hemisphere Survey (UHS) and the release of data which complete the survey's *J*-band coverage. The survey is the product of an evolving collaboration between several international partners. During the period of acquisition of data in this release, these partners have been the UK Science and Technology Facilities Council (STFC), The University of Hawaii, The University of Arizona, Lockheed Martin and the National Aeronautics and Space Administration (NASA).

Survey data were released via the Wide Field Camera (WFCAM; Casali et al. 2007) Science Archive[1] (WSA; see Hambly et al. 2008) on 2017 August 1. This release is initially to UK, University of Hawaii and University of Arizona astronomers. A world-wide release will occur in 1 yr. The release incorporates all data observed from 2012 May 19 up to and including 2017 January 31. This constitutes ∼12 700 deg^2 of *J*-band imaging and associated source catalogue products reaching a median depth of 19.6 mag (Vega) and containing approximately 500 million detected sources.

The aim of the UHS is to provide continuous coverage in the Northern hemisphere in the *J* and *K* bands over the declination range of $0^\circ \leq \delta \leq 60^\circ$, this upper limit being set by UKIRT's mechanical constraints. This goal is achieved by surveying the area within this declination range that is not already covered by the three large area surveys carried out within the UKIRT Infra-red Deep Sky Survey (UKIDSS; Lawrence et al. 2007) programme. These three surveys are the Large Area Survey (LAS) covering an area of ∼3700 deg^2, the Galactic Plane Survey (GPS; Lucas et al. 2008) which covers ∼2100 deg^2 along the northern and equatorial Galactic plane and the Galactic Clusters Survey (GCS) with an area of ∼400 deg^2. Together, the LAS, GPS and GCS provide ∼5200 deg^2 of the full UHS area[2].

The coverage of the UHS (see Section 2.1 and Fig. 2) complements that of the Visible and Infrared Survey Telescope for Astronomy (VISTA) Hemisphere Survey (VHS; McMahon et al. 2013) which covers ∼18 000 deg^2 in the Southern hemisphere in *J* and K_s to similar depths as the UHS. The combination of UHS and VHS comprises an almost complete near-infrared sky survey ∼4 mag deeper than the Two-Micron All-Sky Survey (2MASS; Skrutskie et al. 2006), thus giving rise to a long-term legacy data base. In addition, the *Wide-field Infrared Survey* (*WISE*) all-sky catalogue (Wright et al. 2010) which extends to mid-infrared wavelengths and the optical coverage provided by both the Panoramic Survey Telescope & Rapid Response System (Pan-STARRS) survey (Chambers et al. 2016) and the Sloan Digital Sky Survey (SDSS; see SDSS Collaboration et al. 2016, for the 13th data release) realize an extremely powerful set of surveys covering two decades in wavelength and with well-matched sensitivities.

The layout of this paper is as follows. In Section 2, we outline the survey geometry, observing strategy, pipeline processing, calibration and how the survey products are archived and accessed at the WSA. Section 3 details the data products made available along with supplementary information specific to this release. Information on data quality control (QC) procedures and characteristics of the data is given in Section 4. Finally, we summarize in Section 5. All magnitudes quoted in this paper are Vega magnitudes in the system described by Hewett et al. (2006).

[1] http://wsa.roe.ac.uk

[2] Note that the LAS extends to declinations <0° and that there is an overlap in coverage between the LAS, GCS and GPS.

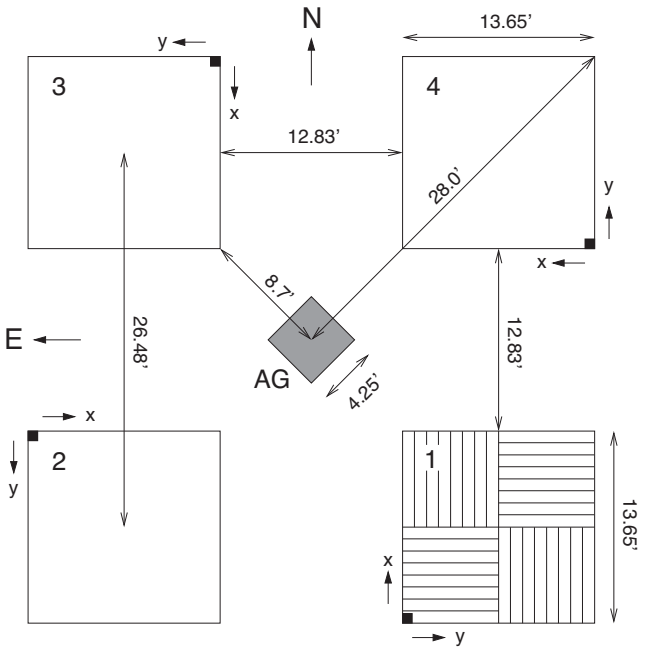

Figure 1. The WFCAM focal plane showing the four detectors and the autoguider (AG). Numbering of detectors is the same as that used in the WSA and for extension numbering in the multi-extension FITS image files. Detectors are divided into four quadrants, each quadrant having eight channels as illustrated in detector 1. Note the convention used for the image pixel coordinate system in each detector. In this figure taken from Dye et al. (2006), north is upwards and east is to the left.

2 SURVEY DESIGN

UKIRT is an infrared-specific telescope with a primary mirror of diameter 3.8 m. Together, UKIRT and WFCAM offer an impressive étendue of ∼2.4 m^2 deg^2, defined as the product of the telescope collecting area and the solid angle of the camera's field of view (FOV). This, combined with low observing overheads due to the high efficiency of WFCAM and a fast tip-tilt secondary mirror on UKIRT which allows dither offsets within 10 arcsec to be carried out without slewing the telescope, makes a highly optimized infrared survey facility.

In this paper, we adopt the nomenclature used by UKIDSS. Accordingly, an *Exposure* is a single 10 s integration which gives rise to a single data file comprising the four separate detector images. The stack of four 10 s Exposures results in a *Stack* frame. The centres of the detector images in an Exposure or Stack frame are offset from the 'base-position' at the frame centre by 18.72 arcmin in NE, NW, SE and SW directions. We use the term *Tile* to designate the contiguous square area formed by positioning four Stacks in a square 2 × 2 grid of spacing 13.24 arcmin (see below). We maintain capitalization hereafter to indicate instances of these specific definitions.

Fig. 1 (taken from Dye et al. 2006, for completeness) shows the layout of the focal plane of WFCAM. An optical charge coupled device acting as the autoguider lies at the centre of the focal plane. The four square 2048 × 2048 pixel detectors are spaced at 94 per cent of the 13.65 arcmin angular width they subtend on the sky. This gives an areal coverage of 0.21 and 0.79 deg^2 per Exposure and per Tile,

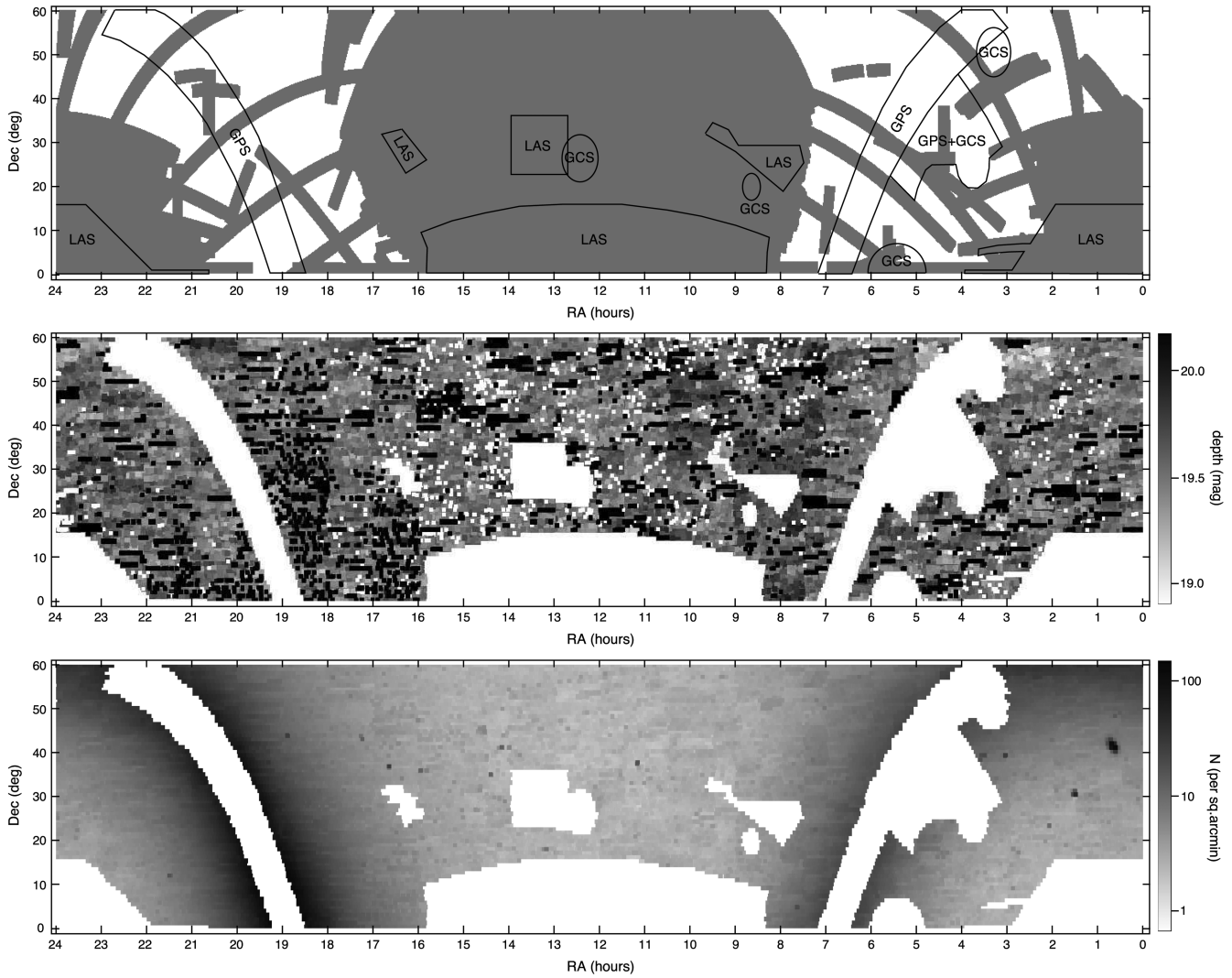

Figure 2. Top: Survey Geometry. The UHS covers the full area plotted, with the 'rUHS' area (constituting the present release) being defined as that area not covered by the UKIDSS LAS, GPS or GCS regions as indicated. Coverage of imaging in SDSS DR13 (SDSS Collaboration et al. 2016) is also plotted in grey for a comparison. Middle: a map of 5σ J-band point source sensitivity in rUHS. Black squares indicate multiframes that have been imaged at least twice and white squares indicate multiframes not included in the standard release products (see Section 3.4 for more details). Bottom: number density of sources detected in all multiframes in rUHS, including the extended release products.

respectively. Readers are referred to Casali et al. (2007) for further technical details regarding WFCAM.

2.1 Geometry and tiling

The UHS geometry is plotted in Fig. 2 which shows the existing area covered by the LAS, GPS and GCS. Hereafter, we refer to the area not covered by these UKIDSS surveys as 'rUHS', the 'r' designating the 'remaining' area.

The rUHS area was tiled using a bespoke piece of software called the Survey Definition Tool (SDT) originally developed for UKIDSS. The SDT forms a contiguous area by overlapping Tiles in right ascension (RA) and declination with a nominal overlap of ∼0.5 arcmin in both directions, set to match the overlap between Exposures within a Tile. Tile placement is also constrained by the availability of good guide stars which must lie within the area of sky subtended by the autoguider's FOV and be within user-defined magnitude limits. For the rUHS, these magnitude limits are $11.0 < B_J < 16.5$ in photographic B_J-band which has an effective wavelength of ∼470 nm. If a suitable guide star is not identified for all four Exposures within a Tile, then the SDT attempts to backtrack in RA to find one. This results in the full Tile overlapping its neighbouring Tile by >0.5 arcmin. Backtracking can continue until the Tile overlaps its neighbouring tile by 75 per cent. If this backtracking still does not result in finding a guide star, the SDT attempts to place two Tiles back at the nominal RA but one at a higher declination and one at a lower declination than the nominal declination. These are given the designation 'north' and 'south' (stored as the `object` attribute of table Multiframe in the WSA – see Section 3.3). If guide stars are still not found, then these two Tiles are backtracked until one is.

This scheme proves successful for the rUHS geometry with all Tiles being assigned guide stars without leaving any areas uncovered. However, the SDT selects its guide stars from version 2.2 of the *Hubble Space Telescope*'s guide star catalogue (Lasker et al. 2008) where a small fraction of sources are actually compact galaxies. These compact galaxies prove problematic for the autoguider which cannot reliably locate their centroid. To determine occurrences of

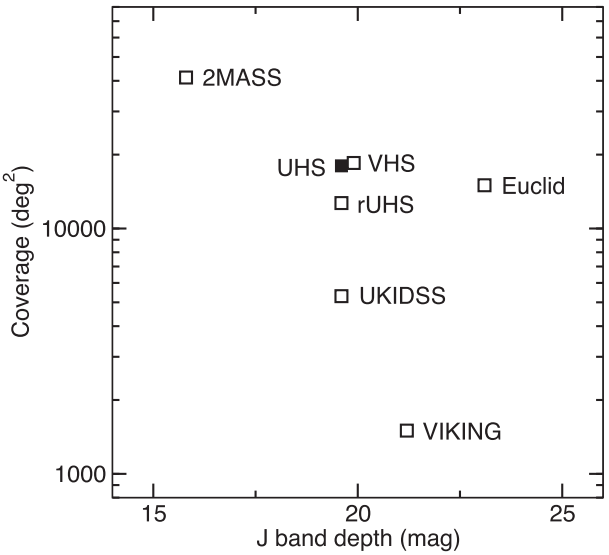

Figure 3. A comparison of 5σ point source sensitivities and coverage of completed, ongoing and forthcoming large-area (i.e. $>1000\,\mathrm{deg}^2$) near-IR surveys. Statistics are shown for 2MASS, UKIDSS (LAS+GPS+GCS), VHS, the VISTA Kilo-degree Infrared Galaxy survey (VIKING; Edge et al. 2013) and the Euclid wide area survey (survey parameters taken from Racca et al. 2016) as well as the UHS and rUHS. The UHS has almost the same areal coverage as the VHS, but in the opposite hemisphere.

compact galaxies, the SDSS was used where possible and when not, the *WISE* all-sky survey catalogue and the 2MASS catalogue were used. It was found that the incorrectly selected compact galaxies tend to have red $J-K$ 2MASS colours and lie redwards of the stellar locus in the *WISE* colour $m(3.4\,\mu\mathrm{m})-m(4.6\,\mu\mathrm{m})$. Appropriate colour thresholds therefore identified the majority of contaminating compact galaxies which were replaced manually, occasionally requiring Exposure frames to be offset from their nominal position within problematic Tiles. Despite these efforts, a small fraction of compact galaxies have remained within the selection of guide stars and this is evident from the measured increase in the fraction of images that have failed due to trailing with increasing galactic latitude (see Section 4.2).

Tiling of the rUHS area was carried out by initially tiling the complete Northern hemisphere up to a declination of 60° and then removing Tiles coincident with those of the LAS, GPS and GCS as defined in the 13th UKIDSS data release. This was carried out in such a way as not to leave any gaps at UKIDSS boundaries. The rUHS area requires ∼16 500 Tiles for complete coverage, which, allowing for overlaps between Tiles, constitutes an area of $\sim 12\,700\,\mathrm{deg}^2$. Fig. 3, shows a comparison of the depth and area of rUHS with existing and forthcoming large surveys. For scheduling purposes, the rUHS area is split into 24 projects, each project spanning one hour in right ascension. Project names appear as the attribute `project` in the `Multiframe` table in the WSA.

2.2 Observing strategy

Observations are divided into 'minimum schedulable blocks' (MSBs). Each rUHS MSB has an execution time of approximately 30 min, designed to be short enough to maintain flexibility of scheduling with other projects at UKIRT but long enough to obtain a sufficient number of observations for generation of the sky subtraction frame (see Section 2.3). This ensures that MSBs are self-contained. MSBs typically complete eight Tiles totalling an on-sky integration time of 1280 s and therefore an overall overhead fraction of 28 per cent due to telescope slewing and detector read-out and flushing (see Lawrence et al. 2007).

MSBs are only executed if the site quality criteria are met. For the rUHS, these are a maximum J-band sky brightness of 15.5 mag arcsec^{-2}, a maximum full width at half-maximum (FWHM) of the point spread function[3] (PSF) of 1.2 arcsec and the requirement that conditions are photometric. The quality of observations can fall outside these criteria if, for example, conditions deteriorate after commencing an MSB but separate QC procedures result in the removal of poor quality data (see Section 4.1).

Observations comprise four 10 s Exposures, each offset in a rhombic dither pattern, which, at the largest extent, measures 6.4 arcsec across. This matches the dither pattern used by the LAS in bands Y, H and K and results in Exposure frames with whole-pixel offsets which are stacked to make a Stack frame. As in the original UKIDSS surveys, 10 s exposures are motivated by reaching a compromise between several different considerations, such as being short enough to allow multiple exposures for median filtering and to minimize saturation by bright sources, but long enough to reduce the contribution of read noise to photometric errors. 10 s Exposures also maintain a relatively low observing overhead.

We note that the J-band strategy adopted by the rUHS does not match the J-band strategy used for LAS observations which were micro-stepped (see Dye et al. 2006). There are therefore no interleaved frame types in the WSA for rUHS data and so images have the native WFCAM pixel scale of 0.4 arcsec. Since the median PSF FWHM is 0.75 arcsec in this release, approximately half of all images exceed the Nyquist sampling limit. We also note that the rUHS does not include any bad weather regions which in the LAS were compensated for by adjusting exposure times. Following the UKIDSS LAS, GPS and GCS, J-band observations use WFCAM's correlated double sampling read mode. The procedure starts with a detector reset and then an initial read. After the desired length of exposure (i.e. 10 s for rUHS), a final read is made and the difference between the two reads constitutes the detected flux, output as counts by the analogue-to-digital converter.

The 24 rUHS projects are scheduled automatically by the observing management system at UKIRT. Priorities between projects are set both dynamically by their airmass and statically using a priority assigned by the project scientist to ensure an approximately uniform rate of completion across projects. In addition to the 24 predefined projects, a 25th 'patch-up' project exists with the highest priority. The purpose of this patch-up project is for the reinstatement of failed observations as identified by the pipeline processing. Reinstatement of projects takes an average time of approximately two months from initial acquisition to re-scheduling, hence the affected Tiles are typically still observable. A whole Tile is reinstated to ensure a sufficient number of Exposures for the sky correction frame. This 'QC-on-the-fly' is a separate process from the bulk QC performed prior to data release (see Section 4.1).

2.3 Pipeline data processing

The data pipeline follows the UKIDSS model where processing is carried out in two stages using the VISTA/WFCAM data-flow system (Irwin et al. 2004; Hambly et al. 2008). In the first stage,

[3] Due to optical aberrations and imperfect alignment between components within WFCAM, the delivered image PSF FWHM of 1.2 arcsec actually corresponds to an intrinsic seeing of ∼1.15 arcsec.

discussed in this section, raw survey data are electronically transferred from UKIRT to the Cambridge Astronomical Survey Unit (CASU). Here, processing removes instrumental signatures from the individual Exposures, stacks Exposures and extracts sources to produce catalogues for each Stack frame. In the second stage, discussed in Section 2.4, catalogue data are integrated into a seamless survey product and together with the processed image data are ingested into a data base hosted by the WSA.

2.3.1 Image processing

Images are first flattened with the master twilight flat-field which is updated regularly at approximately monthly intervals. Flattened images are subsequently sky subtracted using a sky frame computed as a running average of several median-filtered science frames. These science frames are selected to lie within as narrow a window as possible around the observation being corrected. Sky frame subtraction removes residuals due to scattered light and thermal emission mainly from marks and dirt on WFCAM's field lens. rUHS MSBs contain eight Tiles which usually provide ample science frames for median filtering out sources for the sky subtraction frame. However, in principle, the pipeline allows these science frames to be selected from any observer programme so long as they match by filter and exposure time. This latter requirement ensures that exposure-dependent artefacts are removed from images as effectively as possible although in a few per cent of images, sky subtraction residuals are still visible (see Warren et al. 2007, for further details).

A feature of the detectors in WFCAM is cross-talk which occurs between the eight parallel channels in each quadrant (see Fig. 1). This behaviour is similar across all detectors and produces gradient images in neighbouring channels when very bright and saturated stars are present. Cross-talk images typically induce features at $\sim$1 per cent of the differential flux of the source in adjacent channels, falling to $\sim$ 0.2 and $\sim$ 0.05 per cent in successive channels further out. A cross-talk suppression module removes these artefacts although some residuals may still be present in the case of extremely saturated sources.

The WFCAM detectors also exhibit the phenomenon of latency, often referred to as persistence. The effect leaves a residual signal in exposures taken shortly after previously imaging a very bright, saturated source. This decays with subsequent exposures but because the region of the detector remains the same each time, this can sometimes appear in the sky frame and therefore can manifest itself in the sky-subtracted science frames. Currently, the pipeline does not correct for latency.

2.3.2 Source catalogues

Source catalogues are generated using a source extraction algorithm based on the original procedure outlined in Irwin (1985). This identifies sources by searching for groups of four or more inter-connected pixels which all lie 50 per cent above the local background level. The background is estimated by bilinearly interpolating a grid of sigma-clipped median values that are computed within 64 $\times$ 64 pixel blocks over the image (see Irwin & Trimble 1984, for further details). This background estimate is subtracted prior to source photometry and thus removes slowly varying background gradients.

A comprehensive range of parameters are determined for each extracted source. This includes a suite of fixed aperture magnitudes and, for extended sources, morphologically based aperture magnitudes. Apertures are 'soft-edged', meaning that image pixels bisected by the aperture boundary contribute to the summed flux by the pixel fraction contained within the aperture. Also included is a morphological classification that assigns the probability of a source being a star, estimated using a curve of growth determined from the different fixed aperture fluxes. Finally, an error flag warns of potential problems in the photometry due to issues such as bad pixels within the aperture, channel bias problems (i.e. anomalous offsets between detector channels), proximity to other sources and whether the source is saturated (see Section 3.3). Readers are referred to the schema browser on the WSA for more details and a complete list of parameters.

2.3.3 Photometric calibration

Photometric calibration is carried out by the CASU data reduction pipeline. The calibration is based on the magnitudes of 2MASS stars in the WFCAM photometric system as described in Hodkgin et al. (2009). By matching to stars detected in 2MASS with a positional tolerance of 1 arcsec, each WFCAM detector frame is calibrated by computing the median of all per-star zero-points (see below for their definition). This requires transforming the matched stars' magnitudes from the 2MASS photometric system to the WFCAM system (see Hodkgin et al. 2009). The calibration includes a position-dependent correction applied to all fluxes and magnitudes to allow for the astrometric distortion which results in a variable angular pixel scale (see Section 2.3.4).

The use of WFCAM system magnitudes of 2MASS stars for photometric calibration in the manner outlined is a departure from more traditional schemes that are prone to additional systematic errors whereby standards are observed off-target. The selection of 2MASS stars used in the calibration applies an extinction-corrected colour cut of $0.0 \leq J - K \leq 1.0$ and a signal-to-noise cut of >10. Around 99.9 per cent of detector frames have between 25 and 1000 2MASS stars satisfying these criteria within them. If fewer than 25 2MASS stars are found within a detector, then the colour cut is not applied. This process achieves a photometric accuracy of $\sim$2 per cent, this figure having been established through analysis of repeat measurements within UHS data (see Section 4.2) and combining this with the 2MASS global photometric calibration accuracy of $\sim$1 per cent (Nikolaev et al. 2000).

Zero-points are defined as the Vega magnitude corresponding to a total corrected flux of 1 count s^{-1} and assume an airmass of unity. These are stored in the WSA as the keyword `MAGZPT` in the headers of Flexible Image Transport System (FITS) files and as `photZPCat` in table `MultiframeDetector`. The uncertainties in these quantities are `MAGZPTERR` and `photZPCatErr`, respectively, and include the 2MASS calibration error, the error due to uncertainty in the conversion from 2MASS to the WFCAM filter system and any residual offsets between the detectors (see Hodkgin et al. 2009, for further details). The calibrated and corrected magnitude of a source is therefore related to its observed flux via

$$m = \texttt{photZPCat} - 2.5\log_{10}(\texttt{aperFlux3}/\texttt{expTime}) - \texttt{aperCor3} - \texttt{extCorr} - \texttt{distCorr},$$

where `aperFlux3` is the flux in a fixed aperture of radius 1 arcsec in counts (stored in the WSA source detection table `uhsDetection`; see Section 3.3), `expTime` is the integration time in seconds (stored in `Multiframe`), `aperCor3` is the corresponding aperture correction for point sources to transform to total flux (stored in `MultiframeDetector`),

`extCorr` = 0.05[(`amStart`+`amEnd`)/2-1] corrects the assumption of unit airmass in `photZPCat` (the attributes for airmass, `amStart` and `amEnd` being stored in `Multiframe`) and `distCorr` is the correction for the image distortion, computed from astrometry information in the FITS image data files.

2.3.4 Astrometric calibration

For the astrometric solution, the astrometric distortion introduced by the optics is first removed with a radially symmetric polynomial model centred on the WFCAM focal plane (see Irwin et al. 2004). The distortion introduced by WFCAM introduces a linear scale change of 0.6 per cent at the edge of the FOV compared to the centre. In each detector frame, bright but unsaturated stars are identified and used to determine the transformation to align with 2MASS which itself uses the Tycho system (Hog et al. 2000). For the image data, the world coordinate system is then computed in the ZPN projection (Calabretta & Greisen 2002) and the appropriate keywords written to the multi-extension FITS files.

As with UKIDSS, rUHS astrometry exhibits an expected decrease in precision with increasing Galactic latitude due to a decrease in the number of 2MASS stars available for solution (see Section 4.2 for more details).

2.4 Data archive

The processed images and catalogue products generated by CASU in the first stage of the pipeline are delivered to the Wide Field Astronomy Unit (WFAU) in Edinburgh. At this point, every detector frame has an individual associated catalogue. In the second stage of processing at WFAU, these catalogues are merged into a seamless catalogue product. This procedure merges duplicated sources extracted from overlapping detector frame regions and, although not relevant for the present *J*-only release, also cross-matches sources detected in different wavebands. This preparation of catalogue data includes a thorough quality control phase which we describe in detail in Section 4.

Processed images and merged catalogue products are then ingested into a relational data base hosted by the WSA at http://wsa.roe.ac.uk. The reader is referred to Hambly et al. (2008) for more details on the second stage of the pipeline regarding catalogue preparation as well as the design and structure of the data base. In addition, the WSA web pages provide comprehensive information on how data are stored and accessed. We provide an overview of how to obtain basic data products in Section 3.3.

3 DATA RELEASE PRODUCTS

In this section, we specify the data product types made available in this release and how to access them. Section 4 gives details of the characteristics of the data being released.

UKIDSS survey data are available via the WSA. The rUHS *J*-band data being made available in this release form a distinct, separately queryable data base in the WSA called `UHSDR1`. By early 2018, existing UKIDSS data will have been merged with rUHS data but at the present time, users must execute separate queries within rUHS or UKIDSS depending on the co-ordinates being targeted.

3.1 Image data

Image pixel data can be obtained from the WSA in several ways. Menu-driven searches allow users to list Exposure and Stack multiframes that coincide with a given position. These can be downloaded as multi-extension FITS data files with the option of being compressed or uncompressed. Similarly, an image cut-out service provides pixel data of a user-defined geometry around an input co-ordinate or an uploaded list of co-ordinates up to a maximum size of 15 × 15 arcmin. Note that unlike some of the *J*-band observations present in the WSA acquired under the UKIDSS programme, there are no interleaved image products and therefore there are no *leavestack* data types for rUHS in the WSA.

Image data may also be obtained using free-form SQL queries. Primarily, this is accomplished by the attribute `fileName` in the table `Multiframe` which directly links to the multi-extension FITS file stored on the server (see Section 4).

The release includes ∼65 200 Stack and ∼261 000 Exposure multiframes which have passed QC criteria. This corresponds to an areal coverage of ∼12 450 deg^2 by Stack frames once overlaps are taken into account, ∼98 per cent of the nominal rUHS area. As we discuss further in Section 3.4, this data release also includes data that have failed the QC criteria. This extended data set covers 99.9 per cent of the rUHS area.

3.2 Source catalogues

Source catalogues can be obtained with a number of different methods. As with access to image pixel data, menu-driven web interfaces allow sources to be searched for within a user specified distance from an input coordinate. The web interface also allows users to upload an external source catalogue for cross-matching against UHS sources.

Free-form SQL queries enable generation of user-specific source catalogues. For example, sources within a given range of RA, Dec, magnitude, size, ellipticity or more complicated combinations of source properties can be selected.

3.3 Access to data products

The relational data base at the heart of the WSA is interfaced via structured query language (SQL). Users can query the data base using direct free-form SQL or menu-driven searches. The menu-driven searches allow users to download the processed FITS image pixel data (for both Exposures and Stacks) and source catalogues by matching to uploaded coordinate data (see Section 3). Free-form SQL queries enable a much greater degree of flexibility and some useful SQL examples for users are given in Dye et al. (2006) and Hambly et al. (2008).

The WSA data base essentially contains a collection of tables. Information on Exposure and Stack multiframes (referred to in the WSA as 'Normal' and 'Stack' multiframes, respectively, both of which comprise an image for each of the four WFCAM detectors as discussed in Section 2.1) is stored in a table called `Multiframe`. This table contains attributes that can be queried, such as the frame type (`frameType`, which for the rUHS will usually be 'normal' or 'stack'), the base co-ordinates of the observation (`raBase`, `DecBase`), the filter used (`filterID`), the airmass (`amStart` and `amEnd`) and the observation date (`dateObs`). `Multiframe` also contains the attribute `fileName` which provides a web link to the processed pixel data stored as a FITS file for direct download. Every Normal and Stack multiframe has the unique attribute `multiframeID` which is common to many other tables in the WSA to allow cross-linking.

Whilst `Multiframe` contains global information common to each of the four detector frames that constitute the Normal or Stack

frame, the table MultiframeDetector gives information specific to each detector frame. MultiframeDetector is linked to the Multiframe table via the attribute multiframeID. Individual detectors are referenced within MultiframeDetector via the extNum attribute (which labels detectors 1, 2, 3 and 4 as 2, 3, 4 and 5, respectively, in alignment with the FITS header labelling). The table holds data on the photometric calibration (see Section 2.3.3) and image quality such as the FWHM of the PSF (given as the attribute seeing), stellar ellipticity (avStellarEll) and the median sky brightness (skyLevel).

Source catalogue data are stored in one of two main tables. The table uhsDetection stores all sources detected in all Stack frames included in the standard release products (i.e. not sources detected in duplicated frames). Although not relevant for this data release, a source detected in multiple passbands will appear multiple times in uhsDetection. In addition, this table will contain more than one entry for the same source if it lies within a region where Stack frames overlap. In contrast, the table uhsSource is constructed by cross-matching between passbands. In this way, a source not located within an overlapping Stack frame region will contain only one entry in uhsSource with multiband photometry. In the present release, this table holds only *J*-band detections. Sources common to two or more overlapping Stack frame regions are matched using a positional tolerance of 2 arcsec and then flagged in uhsSource using the priOrSec flag (see the WSA schema browser for more details). This flagging designates the primary source as that which, first, has the least severe errors (stored for each source in the ppErrBits flag – see below) and, secondly, is furthest from the detector edge. The table uhsSource contains calibrated magnitudes whereas uhsDetection holds both calibrated magnitudes and fluxes. Catalogues use equatorial (J2000.0 equinox), Galactic and SDSS (λ, η) co-ordinates (Stoughton et al. 2002).

Sources contained in both uhsSource and uhsDetection are assigned an error flag to indicate whether there are likely to be problems with the photometry or morphological parameters. In uhsDetection, this flag is the attribute ppErrBits whereas in uhsSource, the flag is given a prefix corresponding to the filter it was detected in, for example, in this data release, only the flag jppErrBits is populated. The flag is used to warn that there are bad or saturated pixels in the flux aperture, that the source lies in a region with poor flat-fielding or within a dither offset of the stacked frame boundary, or that the source may be affected by cross-talk. The WSA schema browser gives further details.

Within the data base, every source has an associated neighbour table to allow more sophisticated matching algorithms, for example, to identify moving sources where multi-epoch observations are available or to determine clustering statistics. This is implemented by the uhsSourceNeighbours table which has been generated by matching uhsSource to itself and recording all neighbours within 10 arcsec for every source. Sources can also be matched to external source catalogues. A selection of tables has been constructed in the WSA to allow such cross-matching. For example, uhsSourceXDR13PhotoObj and uhsSourceXwise_allskysc match to SDSS DR13 (SDSS Collaboration et al. 2016) and *WISE* (Wright et al. 2010), respectively.

3.4 Data release specifics

Included in this release are additional image and source catalogue data that have not been used to generate the standard release products (uhsSource and uhsDetection). These 'extended release' data products fall into one of two categories. The first is data that have not met QC criteria, mainly due to a poor PSF FWHM and/or a poor depth (see Section 4.1 for more details). The second is data that may or may not have passed the QC criteria but have been excluded from the standard release products because they are repeat observations and their inclusion in the archive ingest process causes significant delay due to the triggering of deep stacking, source extraction and ingestion. (A later data release will include deep stacking of these repeat areas.) This second category is primarily due to repeat observations that have been carried out when an MSB has been stopped and restarted by the telescope operator but also a significant fraction (∼30 per cent) were to rectify a problem with incomplete Tiles (see below). In cases where multiple repeat observations at the same base position pass all QC criteria, the deepest Stack and its associated Normal frames were used to generate the standard release products.

The images included in these additional deprecated data are listed within the table Multiframe alongside the standard release image data. All images and catalogue products can be retrieved from the archive using the 'Archive Listing' form. However, other menu-driven WSA searches revert to using the standard products (uhsSource and uhsDetection) which exclude these additional frames. Users must therefore either deselect the 'purge deprecated frames' option when using menu-driven searches or query the archive with free-form SQL to access them. The attribute deprecated in Multiframe and MultiframeDetector is assigned a value of zero if the frame is included in the standard release or, if it has been excluded, a code greater than zero indicating why it has not be included (see the schema browser on the WSA web pages for more details).

To incorporate the sources detected in these additional frames, two extra tables, uhsDetectionAll and uhsSourceAll, have been created. The table uhsDetectionAll contains all sources already held in uhsDetection plus all additional sources detected in the extra deprecated images regardless of whether they have failed QC criteria or not. When querying uhsDetectionAll, the attributes deprecated and ppErrBits indicate whether a source originates from an image included in the standard release or not and why. The table uhsSourceAll includes all sources from uhsSource plus only those additional sources which originate from frames that did not meet the QC criteria. Sources extracted from repeated frames that pass QC are not included in the merging process and thus are not included in uhsSourceAll. Both uhsDetectionAll and uhsSourceAll cannot be queried with menu-driven searches but must be accessed using free-form SQL only.

An issue that arose in the early stages of rUHS operations was that a software bug in the data acquisition system introduced after an upgrade at UKIRT resulted in the formation of incomplete Tiles. The effect was to observe only three out of the four required base positions with one of these randomly being imaged twice. This affected ∼650 Tiles randomly. The bug was corrected on 2012 September 14 and the problem eliminated thereafter. The affected Tiles were re-queued and subsequently re-observed in full. All four base positions of affected Tiles were observed rather than solely the missing base position. This was to ensure a sufficient number of Exposures observed under similar conditions and close together in time for the creation of a good quality sky frame.

Although these repeat frames have not been deep stacked, these additional data are included in the release and in principle offer an increase in depth of ∼0.4 mag over a non-contiguous area of ∼390 deg^2 compared to the nominal depth. Since the incomplete Tile problem also duplicated one base position at random, within

this area of increased depth, approximately 130 deg^2 is deeper than nominal by ∼0.6 mag. In addition to the increase in depth, these repeat observations allow multi-epoch study with a baseline of up to four months.

Fig. 5 shows the areal coverage of all detector frames repeated at least once, as a function of the maximum separation in time between repeats. The figure applies to all repeated data, including re-observations for the incomplete Tile problem and repeats resulting from re-queueing of aborted but partially completed MSBs. These data amount to a total of area of ∼1630 deg^2 with at least two stacked detector frames but including data that have failed QC. If this is limited to data where there are at least two repeated detector frame stacks that have both passed QC, then this area falls to ∼1410 deg^2.

4 DATA CHARACTERISTICS

In this section, we outline the QC criteria applied to the image and source catalogue products released. Section 4.2 summarizes characteristics of the data.

4.1 QC criteria

All rUHS data made available in this release have been quality-checked using a QC process involving three stages. The first and most fundamental stage is an automatic data integrity check that deprecates corrupt data, including any empty detector images or pixel data with damaged metadata.

In the second stage, all images are manually eye-balled. This process identifies any poor-quality images that are not picked up by the quantitative criteria described below. For example, trailed images often give rise to acceptable measurements of PSF FWHM and ellipticity since only a small fraction of the source's flux is typically trailed. Similarly, extreme variation in channel bias or poor sky subtraction is commonly not manifested in quantities such as frame depth or sky brightness measurements. Other problems that eyeballing identifies are poor flat-fielding, poor cross-talk correction and 'disasters' which is a catch-all category for catastrophic failures due to unknown reasons. Features that are ignored in the eyeballing process include satellite trails, diffraction spikes from bright sources, saturated sources, detector latency and small gradients in the background. This latter feature can be ignored since the source extraction process removes local background gradients (see Section 2.3.2).

For this release, eyeballing was shared between a team of nine. Each team member simultaneously viewed all four detector images belonging to a given Stack at a time, for a subset of all Stacks. In this process, poor-quality multiframes with problems discussed previously were flagged. Consistency within the team was verified by assigning each member a common but randomly selected fraction of the data. To further improve consistency, all flagged frames were then re-eyeballed by the project scientist to unflag any frames deemed acceptable and then apply a code to the unacceptable frames to indicate the nature of the failure. In this way, the eyeballing procedure deprecates entire multiframes, not just detector frames. The attribute `deprecated` in table `Multiframe` in the WSA is given the value of the eyeballing failure code which ranges from 60 to 70 inclusive. Similarly, when set, bit number 30 of the flags `ppErrBits` and `jppErrBits` in tables `uhsDetectionAll` and `uhsSourceAll` indicates that a source has been extracted from an image that has not passed eyeballing checks. We note that only data designated as being of type 'disaster' or 'empty frame' are completely removed from the extended data products.

In the third stage of QC, data are subjected to a series of quantitative thresholds. These result in data being rejected at the detector frame level rather than the multiframe level as with eyeballing. For this release, thresholds were applied to PSF FWHM, stellar ellipticity, zero-point and frame depth as follows:

PSF FWHM: The rejection threshold for PSF FWHM is set at 1.4 arcsec as measured from point sources averaged over the entire detector frame. This is greater than the site quality constraint for the PSF FWHM of 1.2 arcsec to allow for slight broadening of the PSF by sub-optimal guiding and also to allow for changes in seeing whilst an MSB is being executed by UKIRT.

Depth: Depth is defined as the total magnitude of a point source for which the integrated flux within a 2 arcsec diameter aperture is detected at the 5σ confidence level. The threshold applied in this release is at a *J*-band magnitude of 19.0 mag corresponding to 0.6 mag shallower than the median value.

Stellar ellipticity: Detector frames with a mean stellar ellipticity (`avStellarEll` in the table `MultiframeDetector`) of >0.2 averaged over the detector frame are rejected. Stellar ellipticity is defined as $1 - b/a$, where a and b are semimajor and semiminor axis length, respectively. This threshold matches that applied in the UKIDSS LAS. Although the value of 0.2 may be regarded as being quite high, as we show in the next subsection, frame depth is not significantly compromised when stellar ellipticity approaches this limit. Values larger than the threshold usually indicate that the data suffer from additional issues and these are typically picked up by the other cuts applied.

Zero-point: The threshold applied to zero-point (`photZPCat` in table `MultiframeDetector`) is set 0.4 mag brighter than modal. This is a relatively loose threshold and for this release corresponds to the limit 22.6 mag. This rejects detector frames with outlying zero-points whilst relying on the depth threshold to provide the primary criterion. The philosophy here is not to cut too severely on a parameter when the depth has not been compromised.

4.2 Data quality

Fig. 4 shows the correlation between depth, PSF FWHM, zero-point, stellar ellipticity and sky brightness for all 305 280 detector frames being released. The plots indicate the thresholds applied at the detector frame level during the QC process and the site quality constraints set for observations (also shown more quantitatively in Fig. 6). As the figure shows, up to the ellipticity cut at 0.2, depth is distributed quite symmetrically about the median value of 19.6 mag, demonstrating that depth is not compromised by minor tracking inaccuracies. In addition, ellipticity only weakly affects image PSF FWHM. However, as expected, depth is strongly correlated with PSF FWHM and sky brightness.

Fig. 6 shows distributions of the quality measurements featured in Fig. 4 along with the thresholds applied in the QC process. The figure additionally shows the distribution of airmass of detector frames. The thresholds reject 0.8 per cent by PSF FWHM, 1.3 per cent by depth and 0.4 per cent by zero-point. The rate of detector frames rejected by the eyeballing process is 1.7 per cent (with ∼80 per cent of this being attributed to guiding failures). Combining all of these (largely mutually inclusive) rejection rates gives an overall rate of 2.3 per cent of data having not met quality requirements. To reiterate, apart from disasters and corrupt data which constitute a negligible fraction, these rejected data are still available to the user via the tables `Multiframe`, `uhsDetectionAll` and `uhsSourceAll` (see Section 3.4).

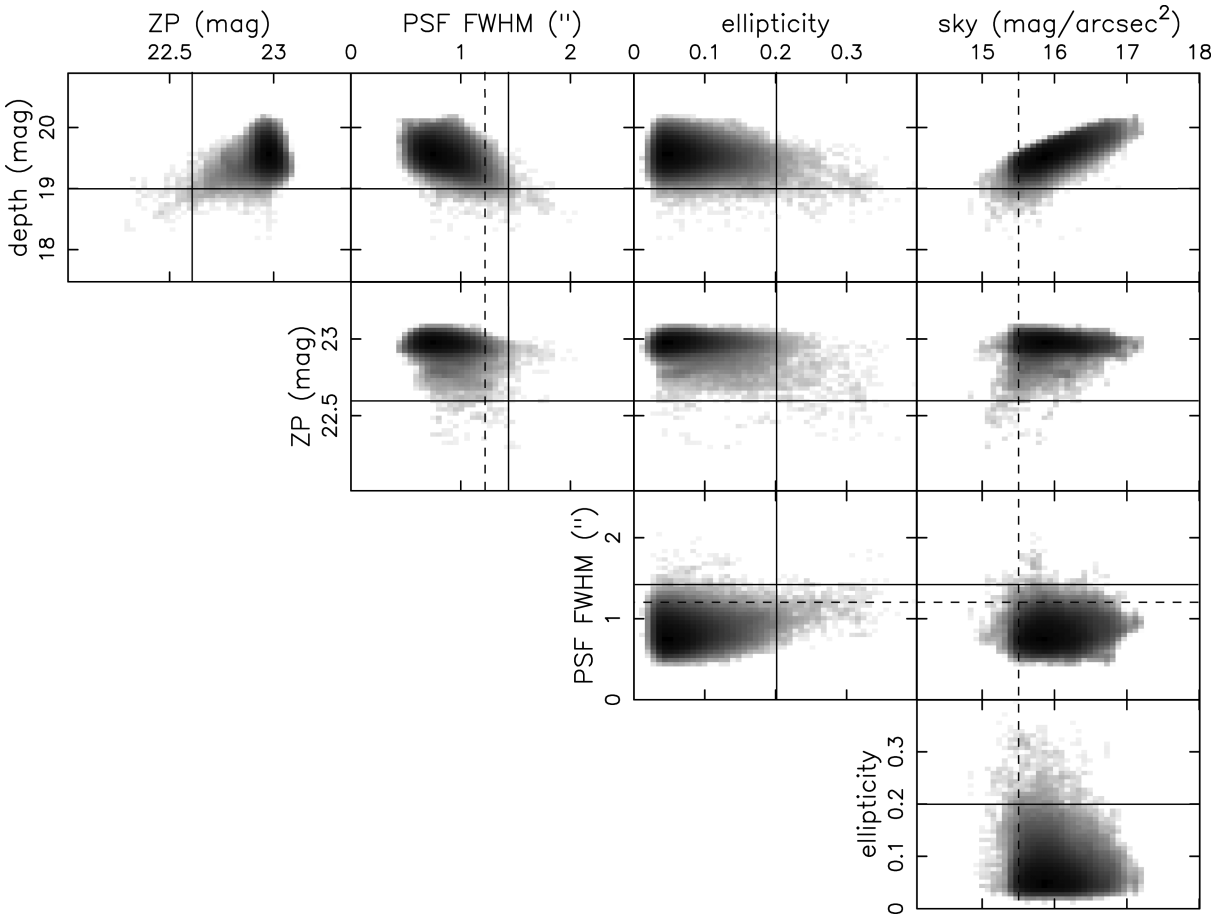

Figure 4. Correlations between data quality measurements for each detector frame in this release. Grey shading shows the logarithm of the number density of detector frames at a given point. Quantities are *J*-band depth (Vega magnitudes), PSF FWHM (arcsec), stellar ellipticity, zero-point magnitude and sky brightness (*J*-band mag arcsec^{-2}). See Section 4.1 for definitions of these quantities. Solid lines indicate the cut applied in the QC process whereas dashed lines show the site quality constraints imposed for observations.

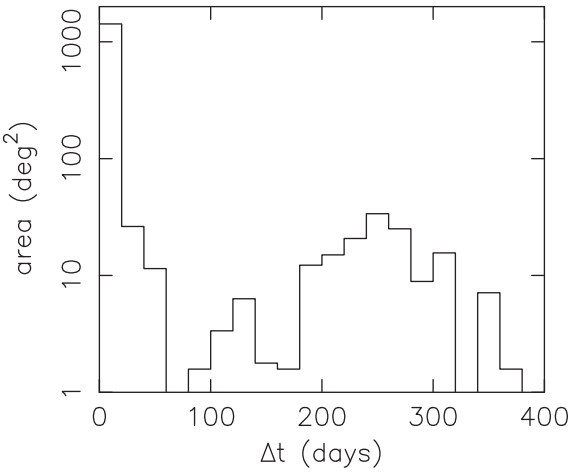

Figure 5. Areal coverage of repeats in this release binned by the time elapsed between the first and last observations within a group of repeat observations. This amounts to a total area of ∼1630 deg^2 and has been computed for all data in the release, including data that have not passed QC but are included in the extended release. Within this, an area of approximately 1410 deg^2 has repeat imaging where at least two of a group of repeats pass QC.

Some of the earlier UKIDSS data releases reported a positive correlation between stellar ellipticity and declination. This was attributed to instrument flexure at a high declination. The remedy implemented for later releases was to compensate for flexure using UKIRT's secondary mirror. Fig. 7 shows the variation of mean stellar ellipticity with declination for data in this release. Whilst there is a slight elevation in ellipticity with increasing declination, this is at a significantly lower level than that reported by UKIDSS and is well within the scatter of ellipticities measured.

Fig. 7 also shows that there is a negligible variation in mean stellar ellipticity with galactic latitude. At higher galactic latitudes, the stellar density falls dramatically, limiting the choice of stars with suitable signal to noise for guiding. This lack of variation therefore shows that the paucity of guide stars at higher galactic latitudes has not noticeably affected the guide quality of QC-passed data. However, the same is not true of the failure rate due to trailed images. The bottom-left panel of Fig. 7 shows the fraction of multiframes that have failed QC by being trailed as a function of their galactic latitude. Here, there is a dramatic increase from almost no frames being trailed at low latitudes to approximately 2 per cent of frames being trailed at latitudes $>60^\circ$. This trend is not seen with declination and hence cannot be attributed to instrument flexure. Instead, the likely dominant cause of these guiding failures is contamination of the selection of guide stars used for rUHS by compact galaxies

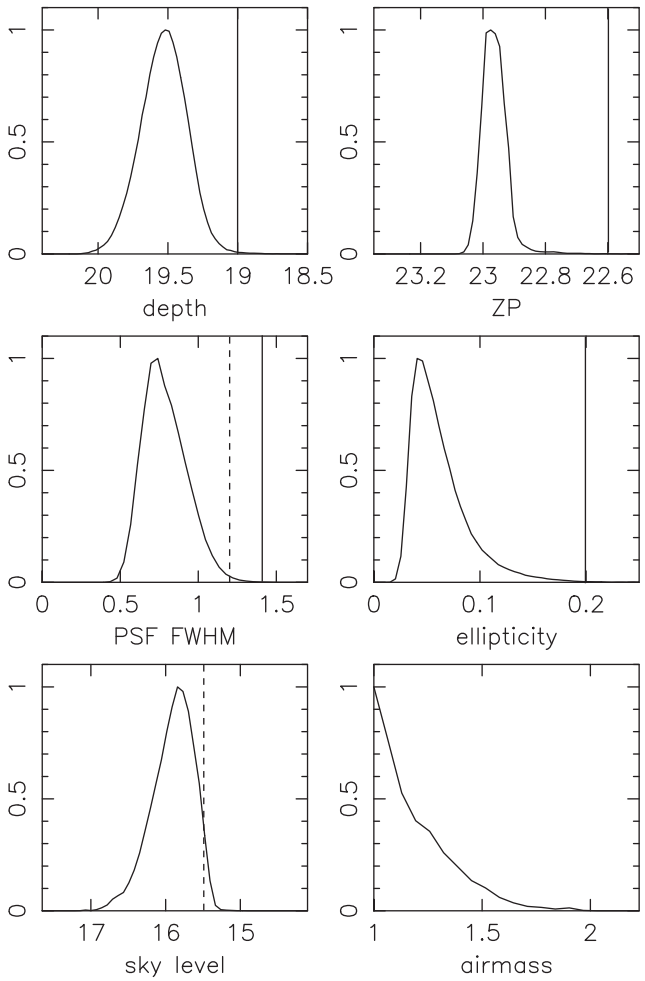

Figure 6. Distributions of data quality measurements for all detector frames in this release. Quantities are *J*-band depth (Vega magnitudes), PSF FWHM (arcsec), stellar ellipticity, zero-point magnitude, sky brightness (*J*-band mag arcsec^{-2}) and airmass. See Section 4.1 for definitions of these quantities. Solid lines indicate the cut applied in the QC process whereas dashed lines show the site quality constraints imposed for observations.

(see Section 2.1) and a stronger occurrence of fainter guide stars at high galactic latitudes.

4.2.1 *Astrometric precision*

The top row of Fig. 8 gives various measures of the astrometric precision of rUHS catalogue data by analysing sources selected from pairs of duplicated detector frames, where both frames in each pair have passed QC criteria (i.e. these are largely the frames that were repeated to patch up incomplete Tiles – see Section 3.4). The plot in the top left of the figure shows how the standard deviation of the separation between matched pairs of unsaturated stars varies with signal-to-noise ratio (SNR). Dividing this by $\sqrt{2}$ gives an estimate of the radius of the circle within which the source centroid can be located with a 1σ confidence (and hence, dividing by a further factor of $\sqrt{2}$ gives an estimate of the 1σ uncertainty in declination or right ascension). The dashed line is the theoretical expectation of the radius of this error circle taken from Ivison (2007) for the median survey PSF FWHM of 0.75 arcsec. This line agrees well with that measured up until an SNR of approximately 100 where a limit in the astrometric precision of 0.01 arcsec is reached due

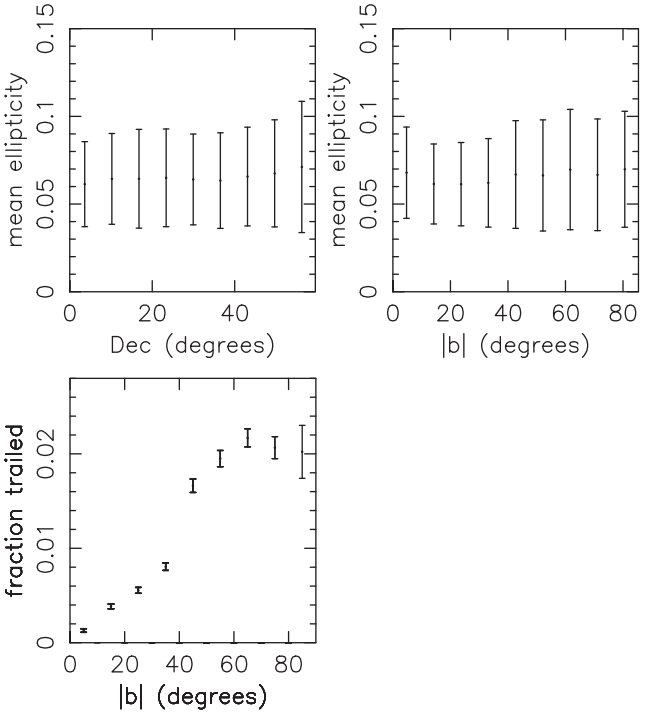

Figure 7. Top left: variation of stellar ellipticity with declination. Error bars show the standard deviation of ellipticity in each declination bin. The plot shows negligible degradation in image quality at a high declination, demonstrating that UKIRT's secondary mirror compensates for instrument flexure well (see the main text for more details). Top right: variation of stellar ellipticity with galactic latitude. Again, negligible variation shows that even at high galactic latitudes (and thus low density of guide stars), guiding quality is maintained. Bottom left: fraction of multiframes that have failed QC by being trailed as a function of galactic latitude. Error bars show Poisson noise.

to the precision with which centroids are determined in the source extraction process.

The middle plot in the top row of Fig. 8 shows how astrometric precision varies with galactic latitude for unsaturated stars selected by $99.5 < \mathrm{SNR} < 100.5$. At low latitudes, the precision is close to the limit of 0.01 arcsec, but this increases monotonically to ~0.03 arcsec by a galactic latitude of $b = 80^\circ$ where there are fewer 2MASS stars with which to determine the astrometric solution. Finally, the plot on the right-hand side of Fig. 8 shows how the mean positional offset between pairs of unsaturated stars located in duplicated frames selected by $99.5 < \mathrm{SNR} < 100.5$ varies as a function of distance from the detector frame centre. The dashed line shows the expected mean offset for the measured astrometric error of 0.01 arcsec for an SNR of 100 taken from the first plot. There is good agreement between the expected and measured mean offset within a radius of 6 arcmin from the centre of the detector frame (~60 per cent of the detector frame area) beyond which, the measured mean offset rises by ~30 per cent. Nevertheless, this is extremely small compared to the global astrometric precision of 2MASS of ~0.2 arcsec (Cutri et al. 2000), demonstrating that systematic errors due to detector edge effects are negligible.

4.2.2 *Photometric precision*

Photometric precision was determined with the same catalogue data used for the astrometric analysis, i.e. unsaturated stars selected from

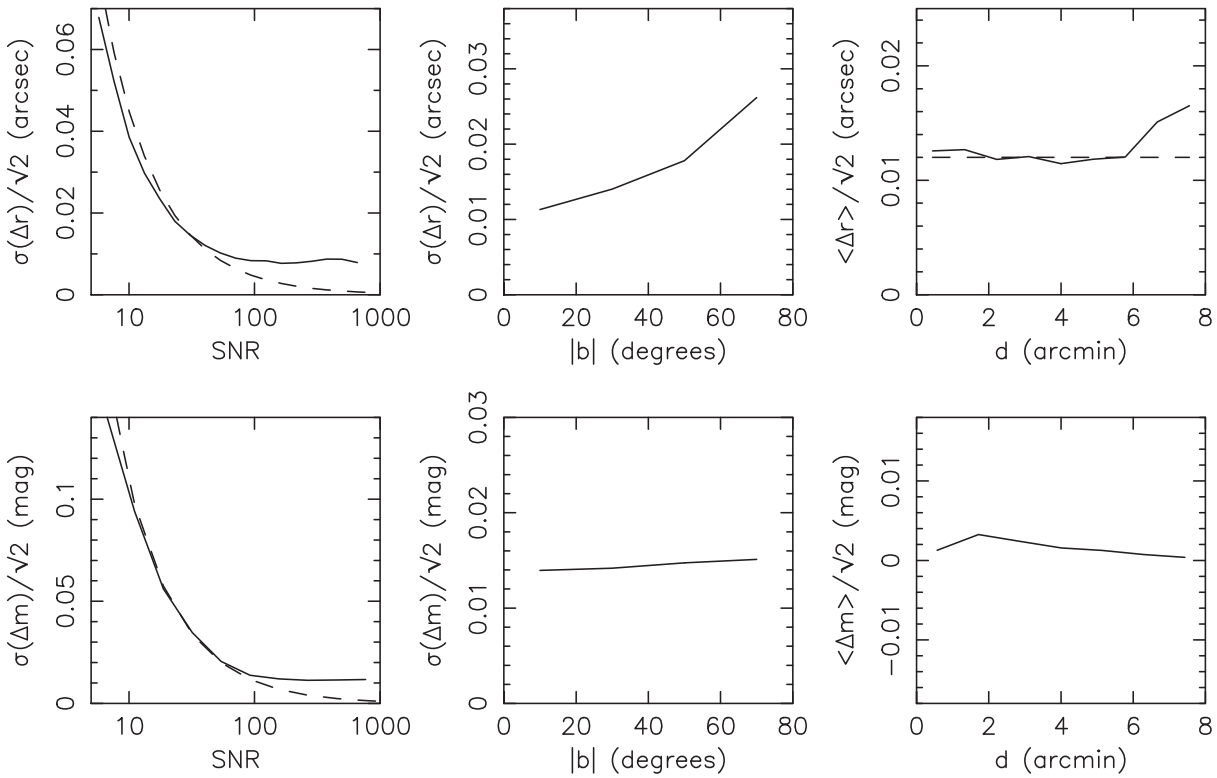

Figure 8. Internal consistency of astrometry and photometry determined from repeat observations. The top row shows how the standard deviation (left and middle plots) and mean (right plot) of the separation, Δr, of unsaturated stars paired between duplicated frames vary as a function of their SNR, galactic latitude and distance, d, from the detector frame centre. Similarly, the bottom row shows the variation in standard deviation (left and middle plots) and mean (right plot) of the magnitude difference, Δm, of unsaturated stars paired between duplicated frames. The dashed line in the top-left plot shows the expected variation in positional precision with SNR as given by Ivison (2007) for a PSF FWHM of 0.75 arcsec. The dashed line in the bottom-left plot shows the theoretical line $\sigma_m = 2.5/(\mathrm{SNR} \times \ln 10)$ for a 1σ error in magnitude, σ_m. The dashed line in the top-right plot shows the expected mean offset for the measured astrometric error of 0.01 arcsec at SNR = 100. For the four plots in the middle and right-hand columns, stars were selected with $99.5 < \mathrm{SNR} < 100.5$.

duplicated detector frames. The bottom row of Fig. 8 shows the results of this analysis. In the bottom-left plot of the figure, the standard deviation of the difference in *J*-band magnitude between matched pairs of stars is seen to vary with SNR in a manner that closely matches the variation expected from simple error propagation [such that the 1σ error in magnitude varies with SNR as $2.5/(\mathrm{SNR} \times \ln 10)$] up to an SNR of 100. At higher SNRs, the photometric precision reaches an asymptotic value of $\simeq$0.01 mag. Combining this limiting internal photometric precision with the global 2MASS precision of $\sim$1 per cent (Nikolaev et al. 2000) gives an absolute photometric precision for the *J*-band data in this release of better than 2 per cent.

The middle plot in the bottom row of Fig. 8 shows that photometric precision is almost consistent across all galactic latitudes, rising only $\sim$15 per cent from low to high latitudes. Similarly, the plot in the bottom-right of Fig. 8 shows negligible systematics in photometric precision due to detector edge effects.

4.2.3 J*-band number counts*

As a final illustration of the extent of the data included in this release, Fig. 9 shows the number counts of galaxies detected in the rUHS in comparison with those determined from the UKIDSS Ultra Deep Survey (UDS; Almaini et al., in preparation). To measure the rUHS galaxy number counts, sources were selected from the WSA table `uhsSource` in a region defined by $|b| > 30^\circ$, being classified by the WSA attribute `jClass` as being non-stellar and being unsaturated according to the attribute `jppErrBits`. It is likely that there is a significant contamination of the resulting rUHS number counts from stars. Quantification of stellar contamination is beyond the scope of such a simple demonstration of dynamic range and is therefore left for future work. For the UDS counts, stars were removed using colour cuts computed using an overlapping $\sim$0.6 deg^2 optically imaged region of the full $\sim$0.8 deg^2 field (details to appear in Almaini et al., in preparation). The error bars plotted allow only for Poisson noise and do not account for variation in PSF FWHM which will affect the 2 arcsec diameter aperture magnitudes used (although the median rUHS PSF FWHM is within 5 per cent of that of the UDS), the inconsistent star–galaxy separation, nor cosmic variance. The UDS galaxy counts at the bright end become discrepant with the rUHS counts since bright galaxies in the UDS catalogue have been removed. Despite the ramifications of these caveats, agreement is very good in the overlap region.

5 SUMMARY

This paper has defined the UHS and the release of $\sim$12 700 deg^2 of new *J*-band survey data. In combination with existing UKIDSS data, this completes the full UHS *J*-band coverage of $\sim$17 900 deg^2, although $\sim$250 deg^2 has failed quality control and will be re-observed within one year of this release.

The newly released data take the form of *J*-band imaging and source catalogue products. A total of approximately 500 million unique sources have been detected, reaching a median 5σ point

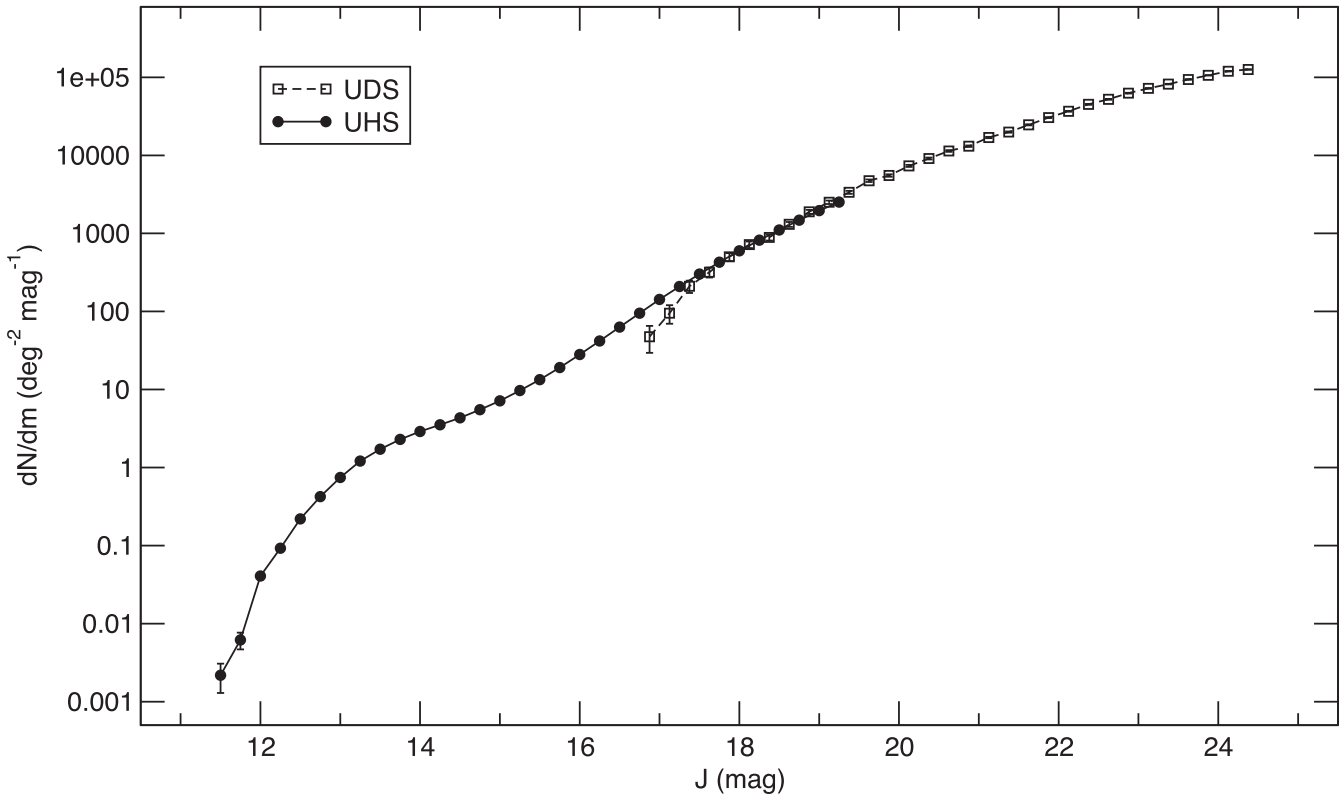

Figure 9. A comparison of *J*-band galaxy number counts from the rUHS data in this release and the UKIDSS UDS DR11 (Almaini et al., in preparation). To determine rUHS galaxy counts, unsaturated sources were selected from a region defined by $|b| > 30^{\circ}$ and classified by the WSA attribute `jClass` as being non-stellar. For UDS, galaxies were distinguished from stars using optical imaging in an $\sim$0.6 deg^2 region of the $\sim$0.8 deg^2 UDS field. Error bars account only for Poisson noise.

source sensitivity of 19.6 mag (Vega) measured within a 2 arcsec diameter aperture. The median PSF FWHM of the new image data products is 0.75 arcsec. In addition, a small, non-contiguous area of $\sim$1630 deg^2 has been repeated, offering an increase in depth by $\sim$0.4 mag over this area. These additional frames have not been deep-stacked in this release but will be provided in a future release.

The data were released via the WSA at wsa.roe.ac.uk on 2017 August 1 to UK, University of Hawaii and University of Arizona astronomers. A world-wide release is scheduled for 2018 August 1. In this present release, the new data are archived in a distinct data base stored at the WSA. In a future release, planned for early 2018, the data will be merged with existing UKIDSS LAS, GPS and GPS data to provide a single, seamless data base spanning a contiguous area in the Northern hemisphere up to a declination of 60°.

At the time of writing, UHS operations are continuing with re-observation of the *J*-band Tiles that failed the quality criteria. Running in parallel with this, *K*-band imaging started in late-July of 2017 at which time survey management was transferred to the United States Naval Observatory. UKIRT is now commencing a more survey-oriented mode of operation and so it is anticipated that the full *K*-band sweep will be completed within a 2-yr time frame.

ACKNOWLEDGEMENTS

SD acknowledges support by the UK STFC's Ernest Rutherford Fellowship scheme. ACE acknowledges support from STFC grant ST/P00541/1. The UHS data in this release have been acquired under an evolving collaboration that has involved the following international partners: STFC, The University of Hawaii, The University of Arizona, Lockheed Martin and NASA. The authors wish to recognize and acknowledge the very significant cultural role and reverence that the summit of Mauna Kea has always had within the indigenous Hawaiian community. We are extremely grateful to have the opportunity to conduct observations from this mountain.

REFERENCES

Calabretta M. R., Greisen E. W., 2002, A&A, 395, 1077
Casali M. et al., 2007, A&A, 467, 777
Chambers K. C. et al., 2016, preprint (arXiv:1612.05560)
Cutri R. M. et al., 2000, Explanatory Supplement to the 2MASS Second Incremental Data Release, available at: https://www.ipac.caltech.edu/2mass/releases/second/doc/explsup.html
Dye S. et al., 2006, MNRAS, 372, 1227
Edge A., Sutherland W., Kuijken K., Driver S., McMahon R., Eales S., Emerson J. P., 2013, The Messenger, 154, 32
Hambly N. C. et al., 2008, MNRAS, 384, 637
Hewett P. C., Warren S. J., Leggett S. K., Hodgkin S. T., 2006, MNRAS, 367, 454
Hodgkin S. T., Irwin M. J., Hewett P. C., Warren S. J., 2009, MNRAS, 394, 675
Hog E. et al., 2000, A&A, 355, L27
Irwin M. J., 1985, MNRAS, 214, 575
Irwin M. J., Trimble V., 1984, AJ, 89, 83
Irwin M. J. et al., 2004, in Quinn P. J., Bridger A., eds, Proc. SPIE Conf. Ser. Vol. 5493, Optimizing Scientific Return for Astronomy through Information Technologies. SPIE, Bellingham, p. 411
Ivison R. J. et al., 2007, MNRAS, 380, 199

Lasker B. M., 2008, ApJ, 136, 735
Lawrence A. et al., 2007, MNRAS, 379, 1599
Liu M. C. et al., 2013, ApJ, 777, L20
Lucas P. W. et al., 2008, MNRAS, 391, 136
McMahon R. G et al., 2013, The Messenger, 154, 35
Marocco F. et al., 2014, MNRAS, 439, 372
Nikolaev S., Weinberg M. D., Skrutskie M. F., Cutri R. M., Wheelock S. L., Gizis J. E., Howard E. M., 2000, AJ, 120, 3340
Racca G. D. et al., 2016, in Mac Ewan H. A., Fazio G. G., Lystrup M., Batalha N., Siegler N., Tong E. C., eds, Proc. SPIE Conf. Ser. Vol. 9904, Space Telescopes and Instrumentation 2016: Optical, Infrared, and Millimeter Wave. SPIE, Bellingham, p. 99040O
SDSS Collaboration et al., 2016, ApJS, preprint (arXiv:1608.02013)
Skrutskie M. F. et al., 2006, AJ, 131, 1163
Stoughton C. et al., 2002, AJ, 123, 485
Wang F. et al., 2017 ApJ, 839, 27
Warren S. J. et al., 2007, MNRAS, 375, 213
Wright E. L. et al., 2010, AJ, 140, 1868
Yang J. et al., 2017, AJ, 153, 184

This paper has been typeset from a TEX/LATEX file prepared by the author.